Microemulsion-Assisted Synthesis of Tunable Superparamagnetic Composites

Pedro Tartaj* and Carlos J. Serna

Particulate Materials Department, Instituto de Ciencia de Materiales de Madrid, (CSIC), Campus de Cantoblanco, 28049, Madrid, Spain

Received May 27, 2002. Revised Manuscript Received July 3, 2002

Tunable superparamagnetic materials have been obtained by the thermal annealing of iron oxide/silica composites synthesized using microemulsions with a high content of the iron oxide precursor. The crystallochemical characteristics of the powders obtained after controlled hydrolysis within the reverse micelle nanocavities and their thermal evolution up to the formation of the γ-Fe_2O_3 crystalline phase were studied. The thermally annealed composites clearly exhibited superparamagnetic behavior with the value of the saturation magnetization easily tuned by changing the iron oxide content and the annealing temperature. Information on the influence of particle size and interparticle interactions on the magnetic properties of the composites was inferred from zero field and field cooling measurements and also from the decay of the reduced remanence with temperature. It was observed that the blocking temperature increased with content and particle size of γ-Fe_2O_3. We have also determined a strong dependence of the effective anisotropy with the particle size associated with the existence of surface anisotropy.

Introduction

Materials containing crystallites or particles of nanometer dimensions have shown interesting properties related to their extremely small size. Quantum states in the nanoparticles are size-dependent, leading to novel mesoscopic properties that are sometimes dramatically different from those of the atomic and bulk counterparts. In particular, when the size of magnetic particles is reduced to a few tens of nanometers, they exhibit a number of outstanding physical properties such as superparamagnetism, giant magnetoresistance, quantum tunneling of the magnetization, and large coercivities.[1]

Magnetic nanoparticles are normally prepared in diamagnetic matrixes to avoid their natural tendency to form aggregates.[2] In particular, those containing γ-Fe_2O_3 nanocrystals are of technological importance because they have potential applications in magnetic-tape media,[3] magnetooptical devices,[4] magnetic refrigerators,[5] and catalysis.[6] Among the different matrixes, silica (SiO_2) seems to have the best characteristics. The silica matrix helps to prevent the conversion of the γ-phase into the α-phase on heating,[7] allowing a fine-tuning with temperature of the magnetic properties.[8] In recent years, special attention has been focused on the use of these composites for chemical separation of, for example, nuclear waste, biochemical products, and cells.[9] Because this application requires the preparation of stable suspensions of the magnetic composites, the ideal microstructure must consist of superparamagnetic nanocrystals dispersed in submicrometer diamagnetic particles that are expected to have long sedimentation times in the absence of a magnetic field.

Also of interest is that the magnetic behavior of these composites can vary widely depending on the size and distribution of the nanocrystalline particles as well as on the volume fraction and on the interaction of the nanomagnets with the matrix.[10] In general, these systems are composed of a collection of different-sized single-domain magnetic particles. All particle moments are blocked at the lowest temperatures; however, with increasing temperature, the smaller particle moments will become superparamagnetic, moments of intermediate-sized particles will undergo collective excitations, and the moments in the largest particles will remain blocked. This wide variety of magnetic behavior is

* To whom correspondence should be addressed. Fax: 34-913720623. E-mail: ptartaj@icmm.csic.es.

(1) (a) Gu, E.; Ahmad, E.; Gray. S. J.; Daboo, C.; Bland, J. A.; Brown, L. M.; Chapman, J. C. *Phys. Rev. Lett.* **1997**, *78*, 1158. (b) Mehn, M.; Punadjela, K.; Bucher, J.; Rousseausx, F.; Decanini, D.; Bartenlian, B.; Chappert, C. *Science* **1996**, *272*, 1782. (c) Martínez, B.; Obradors, X.; Balcells, L. I.; Rovanet, A.; Monty, C. *Phys. Rev. Lett* **1998**, *80*, 181.

(2) Tong, B. Z.; Geng, Y.; Yip Lam, J. W.; Li, B.; Jing, X.; Wang, X.; Wang, F.; Pakhomov, A. B.; Zhang, X. X. *Chem. Mater.* **1999**, *11*, 1581.

(3) Onodera, S.; Kondo, H.; Kawana, T. *MRS Bull.* **1996**, *21*, 235.

(4) Guerrero, H.; Rosa, G.; Morales, M. P.; Del Monte, F.; Moreno, E. M.; Levy, D.; Pérez del Real, R.; Belenguer, T.; Serna, C. J. *Appl. Phys. Lett.* **1997**, *71*, 2698.

(5) McMichael, R. D.; Shull, R. D.; Swartzendruber, L. J.; Bennet, L. H.; Watson, R. E. *J. Magn. Magn. Mater.* **1992**, *111*, 29.

(6) Ida, T.; Tsuiki, H.; Ueno, A.; Tohji, K.; Udagawa, Y.; Iwai, K.; Sano, H. *J. Catal.* **1987**, *106*, 428.

(7) Ennas, G.; Musinu, A.; Piccaluga, G.; Zadda, D.; Gatteschi, D.; Sangregorio, C.; Stanger, J. L.; Concas, G.; Spano, G. *Chem. Mater.* **1998**, *10*, 495.

(8) Tartaj, P.; González-Carreño, T.; Serna, C. J. *Adv. Mater.* **2001**, *13*, 1620.

(9) (a) Bergemann, C.; Müller-Schulte, D.; Oster, J.; Brassard, L.; Lübbe, A. S. *J. Magn. Magn. Mater.* **1999**, *194*, 45. (b) Nuñez, L.; Kaminski, M. D. *J. Magn. Magn. Mater.* **1999**, *194*, 102. (c) Chatterjee, J.; Haik, Y.; Chen, C. J. *J. Magn. Magn. Mater.* **2002**, *246*, 382.

(10) (a) Liu, C.; Zhang, Z. J. *Chem. Mater.* **2001**, *13*, 2092. (b) Katiyar, P.; Kumar, D.; Nath, T. K.; Kvit, A. V.; Narayan, J.; Shattopadhyay, S.; Gilmore, W. M.; Coleman, S.; Lee, C. B.; Sankar, J.; Singh, R. K. *Appl. Phys. Lett.* **2001**, *79*, 1327.

10.1021/cm021214d CCC: $22.00
Published on Web 09/19/2002

further complicated by interparticle interactions[11] arising from the difficulty in controlling particle dispersion. Interparticle interactions (usually of a dipolar nature) will affect the effective anisotropy energy and change the temperature at which a particle becomes superparamagnetic. In this way, the use of chemical routes able to produce magnetic nanoparticles, say γ-Fe_2O_3 nanocrystals, dispersed in a diamagnetic matrix, say silica, could have significant value not only from a technological point of view but also to better understand the magnetic behavior of the magnetic nanocrystals.

Many naturally occurring biological reactions take place in organized media, and the self-organization obtained with surfactants in solution has opened a systematic exploration of their use to control chemical reactions.[12] In nonpolar solutions, certain amphiphilic molecules form aggregates with their polar headgroups pointing to the interior, leading to their description as "reverse micelles".[13] When a small amount of polar solvent (most commonly water) is added, the micelles swell, creating a new, confined liquid phase on the inside. These surfactant-stabilized nanocavities (typically in the range of 10 nm) provide a confinement effect that limits particle nucleation, growth, and agglomeration. Therefore, this method is especially appropriate for the preparation of nanosized powders.[14] Moreover, given that the presence of Fe^{2+} cations is necessary for the formation of the γ-Fe_2O_3 phase,[15] another benefit of the use of microemulsions is the high amount of carbonaceous species present in the process that can act as reducing agents.

The present paper reports a simple and versatile method to prepare submicrometer γ-Fe_2O_3/SiO_2 superparamagnetic composites using microemulsions with a high content of the iron oxide precursor. The composites so obtained have been characterized in terms of phase composition, morphology, and chemical composition. We have also studied the thermal evolution of powders to relate the magnetic behavior of the composites to the particle size and content of the γ-Fe_2O_3 crystalline phase.

Experimental Section

Chemicals. Water-in-oil microemulsions (reverse micelles) were prepared using Igepal CO-520 (Aldrich), Igepal CO-720 (Aldrich), or Triton X-100 (Aldrich) as surfactant. When Triton X-100 was used as surfactant, we also used 1-hexanol (Aldrich) as cosurfactant to stabilize the microemulsion. Cyclohexane (Aldrich, 99.5% anhydrous) dehydrated with molecular sieves was used as the continuous oil phase. Tetraethoxysilane (TEOS, Fluka, 97%), $Fe(NO_3)_3 \cdot 9H_2O$ (Aldrich, 99%), ammonium hydroxide (Aldrich, 29%), and ethanol (Aldrich, 99.5% anhydrous) were used as received. Deionized water was used in all experiments.

Synthesis. The microemulsions were prepared at room temperature by the addition of 2.5 M iron nitrate aqueous solutions to a solution with the surfactant, cyclohexane, and TEOS in the desired proportions. To obtain the microemulsion, the solution was thoroughly shaken for 5 min and then stirred for 4 h to ensure the formation of stable microemulsions. The complete hydrolysis of TEOS and the iron nitrate salt was carried out by adding to the microemulsion an equal volume of a 2 M ammonium aqueous solution. The suspension so generated was kept under magnetic stirring for 24 h and further centrifuged at 10 000 rpm for 1 h. The powder so obtained was washed with $EtOH/H_2O$ five times, further refluxed at 70 °C in EtOH under constant stirring for 24 h, and finally dried at 50 °C overnight. A higher number of washing/centrifugation procedures or longer refluxing times did not affect (as was concluded by the lack of changes in the infrared spectrum) the amount of residual species remaining in the samples.

Characterization Techniques. The different phases present in the solids were assessed by X-ray diffraction (XRD, PW1710, Philips). γ-Fe_2O_3 crystallite sizes were obtained as an average of the three different crystallite sizes values estimated from the line width of the (220), (311), and (400) diffraction lines by using the Scherrer equation. Infrared spectroscopy (IR, 20SXC, Nicolet) was mainly used to determine the presence of residual carbonaceous species coming from the surfactants. To record the infrared spectra, the powders were diluted in a KBr matrix. The morphology of the powders was examined by transmission electron microscopy (TEM, 2000 FX2, JEOL). Elemental analysis of samples was done with an energy dispersive spectrometry analyzer (EDS, Oxford Link 5118) integrated in a scanning electron microscope (SEM, Zeiss DSM 960). Chemical analyses at selected areas of ~20 nm were carried out with an energy-dispersive spectrometry analyzer (QX 2000, Oxford Link) integrated in the TEM.

Magnetic properties of the samples were recorded in a vibrating sample magnetometer (model VT10, Oxford). Saturation magnetization (M_S) and coercivity (H_C) were obtained from the hysteresis loops registered up to a field of 7 T. Saturation magnetization was determined by extrapolating to infinite field the experimental results obtained in the field range where the magnetization increases linearly as a function of $1/H$. The temperature dependence of the magnetization was monitored by zero field cooling (ZFC) and field cooling (FC) experiments. The ZFC curve was obtained by first cooling the system in a zero magnetic field to 5 K. Then a magnetic field was applied (200 G), and the magnetization was measured while the temperature was increased. The FC curve was obtained in a similar way except that the sample was cooled in the measuring field (200 G).

Results and Discussion

Samples Preparation and Characterization. Three samples with different Fe/(Fe + Si) mole fractions, F5S (5%), F10S (10%), and F20S (20%), were prepared. Because the main objective of this work was to obtain a significant amount of powders with a microstructure consisting of submicrometer particles using the lowest possible amount of organic solvent, we first carried out experiments with the surfactant Igepal CO-520. This surfactant was recently reported to be adequate for the preparation of iron oxide-doped alumina nanoparticles from microemulsions containing a high content in iron and aluminum nitrates.[14b] It was found that, for a surfactant concentration of 0.2 M, a maximum value of 0.1 M in iron salt concentration could be used. Higher concentrations, irrespective of the amount of surfactant added, failed to produce stable microemulsions. Under these particular conditions, the hydrolysis of $Fe(NO_3)_3$ and TEOS with NH_3 produced powders that consisted of rounded particles with submicrometer sizes (adequate among others for chemical separation applications) between about 0.1 and 0.7 μm (Figure 1). Changing

(11) Dormann, J. L.; Fiorani, D.; Tronc, E. *Adv. Chem. Phys.* **1997**, *98*, 283.

(12) Fendler, J. H. *Membrane Mimetic Chemistry: Characterization and Applications of Micelles, Microemulsion, Monolayers, Bilayers, Vesicles, Host−Guest Systems and Polyions*; Wiley: New York, 1975.

(13) Luisi, P.; Straub, B. E. *Reverse Micelles*; Plenum: New York, 1984.

(14) (a) Zarur, A. J.; Ying, J. Y. *Nature* **2000**, *403*, 65. (b) Tartaj, P.; Tartaj, J. *Chem. Mater.* **2002**, *14*, 536.

(15) Cornell, R. M.; Schwertmann, U. *The Iron Oxides. Structure, Properties, Reactions, Occurrence and Uses*; VCH: Weinheim, 1996.

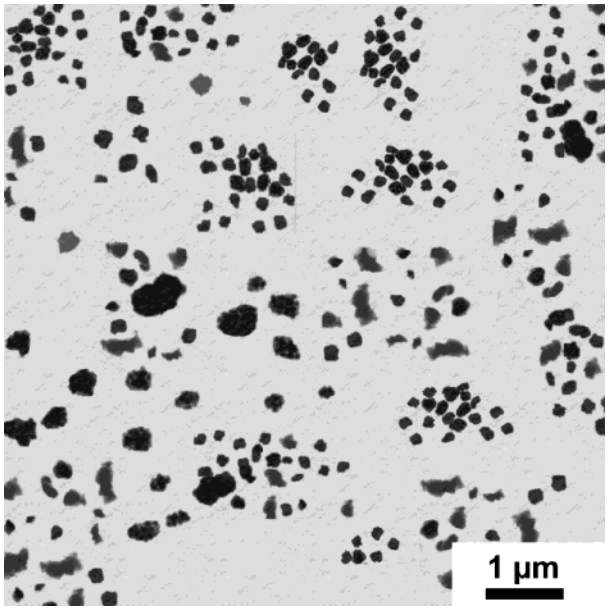

Figure 1. TEM picture of a typical microstructure of the powder obtained after the hydrolysis process.

either the iron salt content in microemulsions (down to a value of 0.025 M),[16] the nature of the surfactant (Igepal CO-720 and Triton X-100), or both, did not significantly affect the microstructure of the obtained powder. This microstructure has certain similarities with the typical ones observed in powders prepared by polymeric sol−gel methods (hydrolysis of TEOS in acid medium) though less massive.[17] It seems that the hydrolysis of Fe^{3+} cations in the initial aqueous solution provides a strong acidic medium within the reverse micelle nanocavities, favoring the condensation of the Si−O−Si species and therefore the trapping of the iron oxide nuclei within the resulting silica network. The confinement effect supplied by the surfactant is probably responsible for partial control of the aggregation process, driving to composites constituted by submicrometer particles.

Irrespective of the size of the aggregates, the microchemical analysis carried out in selected areas of ∼20 nm showed a chemical composition similar to the average composition of powders (high compositional homogeneity). The IR spectrum of samples (not shown) displayed the presence of residual carbonaceous species, which indicates that the washing procedure was not sufficient to remove all the organic residues. More effective methods to remove the residual organic species were not examined because as already mentioned the presence of a certain amount of carbonaceous species favors the formation of the γ-phase instead of α-Fe_2O_3.

The samples obtained after the hydrolysis were amorphous to XRD. After heating the powders at 900 °C (F5S900, F10S900, F20S900), diffraction peaks at 30.3, 35.7, and 43.3° associated with the presence of cubic γ-Fe_2O_3 phase[18] with a similar crystallite size (∼3 nm) were observed (Figure 2, Table 1). At this temperature, no evidence of the presence of α-Fe_2O_3 (absence of the main diffraction line at 33.2°) and ϵ-Fe_2O_3 (absence of the main diffraction line at 38.3°) was observed.[19] The only significant contribution could come from the presence of Fe_2SiO_4,[20] which has the main diffraction line located at the same position as that of the main diffraction line of the γ-Fe_2O_3 phase; however, the fact that the second most intense diffraction line at 31.6° always appears at higher angles with respect to the diffraction peak centered at 30.3°, and especially the absence of diffraction lines at 38.9°, seems to also disregard the presence of this phase. Supporting this result, the γ-Fe_2O_3 crystallite sizes determined from the line width of the three diffraction lines displayed in Figure 2 were similar, which seems to confirm that in

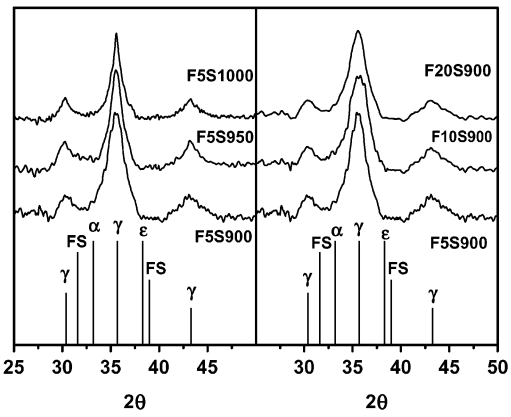

Figure 2. X-ray diffraction patterns showing the presence of γ-Fe_2O_3 in all samples. The main diffraction lines of the α-Fe_2O_3, ϵ-Fe_2O_3, and Fe_2SiO_4 (FS, in this case the second and third most intense lines because the most intense one would appear overlapped with the main one of the γ-Fe_2O_3 phase at 35.7°) along with the diffraction lines of the γ-Fe_2O_3 phase are also represented. As observed, the presence of α- and ϵ-Fe_2O_3 phases can be disregarded. Meanwhile, the absence of diffraction peaks at 38.9° and the fact that the peak at 31.6° always appears at higher angles with respect to the diffraction peak centered at 30.3° seem to confirm the absence of Fe_2SiO_4.

Table 1. Molar Fraction, Fe/(Fe + Si), Crystallite Size (D_{XR}) Determined as an Average of the Three Different Crystallite Sizes That Can Be Obtained from the Line Width of the (220), (311), and (400) Diffraction Lines by Using the Scherrer Equation, Particle Diameter from the TEM Pictures Supposing a Log-Normal Distribution (D_{TEM}), Magnetic Size (D_{Mag}) Determined Following the Method of Chantrell et al.,[23] and M_S (Normalized to the Iron Oxide Content) at Room Temperature

sample	molar fraction (%)	D_X (nm)	D_{TEM} (nm)	D_{Mag} (nm)	M_S (emu/g of Fe_2O_3)
F5S900	5	3.4 (0.3)	3.0 (0.3)	3.1 (0.3)	28
F5S950	5	4.5 (0.5)	3.9 (0.5)	3.9 (0.4)	41
F5S1000	5	5.3 (0.5)	4.9 (0.5)	5.1 (0.4)	52
F10S900	10	3.2 (0.2)	3.0 (0.4)	3.2 (0.3)	30
F20S900	20	3.4 (0.3)	3.2 (0.4)	3.0 (0.4)	26

(16) No additional experiments were carried out at lower iron salt concentrations because in order to obtain a significant amount of powder we would need to use a high amount of organic solvent.

(17) Del Monte, F.; Morales, M. P.; Levy, D.; Fernandez, A.; Ocaña, M.; Roig, A.; Molins, E.; O'Grady, K.; Serna, C. J. *Langmuir* **1997**, *13*, 3627.

(18) JCPDS file 39-1346. The γ-Fe_2O_3 structure here detected most likely belongs to the space group $Fd3m$, in accordance with a face-centered cubic lattice (Pecharromán, C.; González-Carreño, T.; Serna, C. J. *J. Solid State Chem.* **1994**, *108*, 158). Below ∼5 nm, it has been observed that vacancy-disordered γ-Fe_2O_3 belonging to this space group is the most likely phase to be detected (see ref 22). In accordance, values of the cell parameter a of ∼8.40 Å, similar to that determined for a vacancy disordered γ-Fe_2O_3 (see ref 15), were estimated for the samples. However, the low content in iron oxide of the samples precludes definitely disregarding the presence of a superstructure because superlattice reflections could be lost in the background noise.

(19) JCPDS files 33-0664 and 16−0653.

(20) JCPDS file 34-0178.

the samples no other crystalline phases that could be hidden within the broad lines associated with γ-Fe_2O_3 are present. Moreover, this result is in agreement with previously published works,[7,17,21] which observed that, in the iron oxide/silica system, the γ-Fe_2O_3 phase is stabilized at very small particle sizes (below about 10−15 nm), while the other crystalline phases are detected for bigger iron oxide particle sizes normally generated after heating the composites at high temperature. The heating also generated a weight loss of ∼20 wt % associated with the release of both adsorbed water (100 °C, ∼5 wt %) and residual carbonaceous species coming from the incomplete elimination of the surfactant (550 °C, ∼15 wt %). However, below 900 °C, we did not observe any crystalline phase by XRD, probably due to the small particle size of the generated nanocrystals (with a grain size lower than ∼2 nm, diffraction effects are diffuse and close to the background noise). No detailed characterization was made in these samples because, for such a small particle sizes, very low values of the saturation magnetization are expected,[22] which precludes the use of the composites for magnetic applications.

The XRD of the sample with the lowest iron oxide content (F5S) heated at 950 (F5S950) and 1000 °C (F5S1000) displayed diffraction peaks associated with the γ-phase, the crystallite size of which increased with temperature (Figure 2, Table 1). Arguments similar to that previously mentioned to disregard the presence of other crystalline phases such as α-Fe_2O_3, ϵ-Fe_2O_3, and Fe_2SiO_4 phases can be applied to disregard the presence of these phases in samples F5S950 and F5S1000 (Figure 2). The onset of the γ- to α-transformation took place at 1050 °C (data not shown). The transformation temperature was observed to decrease as the iron oxide content in samples increased (1000 and 950 °C for samples F10S and F20S, respectively). Thus, the amount of iron oxide in the composites and the temperature determined the relative content of α-Fe_2O_3/γ-Fe_2O_3. Given that an increase of the crystallite size favors the γ- to α-phase transformation,[7] it was not surprising that samples with the highest iron oxide content (shorter diffusion distances between Fe_2O_3 nuclei) were enriched in the α-form.

TEM micrographs carried out in the samples heated between 900 and 1000 °C showed the presence of particles of a size similar to that observed in the initial samples, but now the presence of γ-Fe_2O_3 nanocrystals (black spots), of a size similar to that determined by XRD, distributed throughout a silica matrix can be clearly observed (Figure 3, Table 1). This result seems to confirm that indeed the initial microstructure of the powders is the result of a typical sol−gel process though confined by the presence of the reverse micelles. In accordance with XRD, the γ-Fe_2O_3 particle size in sample F5S increased with temperature (Figure 3, Table 1). Also, it is clearly observed that the γ-Fe_2O_3 particle size in samples F5S and F20S heated at 900 °C was similar, with the separation distance between particles

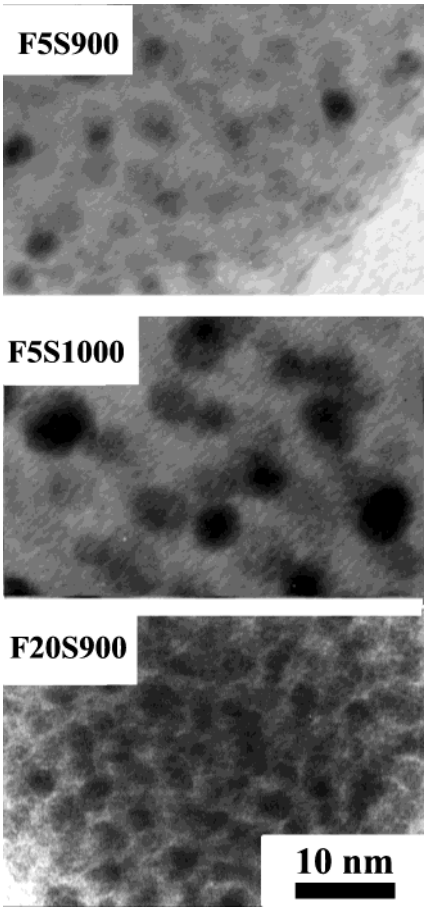

Figure 3. Details of the microstructure of sample F5S heated at 900 and 1000 °C, and sample F20S heated at 900 °C. The dark spots correspond to γ-Fe_2O_3 nanocrystals. Note both how the γ-Fe_2O_3 particle size increases with temperature and how the separation distance between particles decreases with the increase in iron oxide content. The scale bar is the same for all the pictures.

decreasing with the increase in iron oxide content. It is also clear that, as expected, the size dispersion increased with both the iron oxide content and the heating temperature (Table 1). Also, the similarity of sizes obtained by both TEM and XRD seems to confirm that indeed the main crystalline phase present in the composites is γ-Fe_2O_3.

Magnetic Behavior. The magnetic characterization was performed in powders, in which γ-Fe_2O_3 was the only crystalline phase. Size effects (Table 1) were studied for samples F5S900, F5S950, and F5S1000. Interaction effects were examined in samples F5S900, F10S900, and F20S900 that have similar crystallite size (Table 1). Superparamagnetic behavior (i.e., zero coercivity field) was always observed for all samples at room temperature (data not shown). The M_S values, were, in all cases, lower that that of bulk γ-Fe_2O_3 (75 emu/g), which reflects the small particle size of the γ-Fe_2O_3 (Table 1). Surface and finite size effects have been reported as being responsible for the anomalous magnetic behavior manifested by nanoparticles.[22] Spin canting at the surface, the interior of the particles, or both, produces a reduction in saturation magnetization values.[22] Supporting this interpretation, M_S values increased with the crystallinity (sample F5S heated at different temperatures, Table 1), and for the samples

(21) (a) Chaneac, C.; Tronc, E.; Jolivet, J. P. *Nanostruct. Mater.* **1995**, *6*, 715. (b) Chaneac, C.; Tronc, E.; Jolivet, J. P. *J. Mater. Chem.* **1996**, *6*, 1905.

(22) Morales, M. P., Veintemillas-Verdaguer, S.; Montero, M. I.; Serna, C. J.; Roig, A.; Casas, Ll.; Martinez, B.; Sandiumenge, F. *Chem. Mater.* **1999**, *11*, 3058.

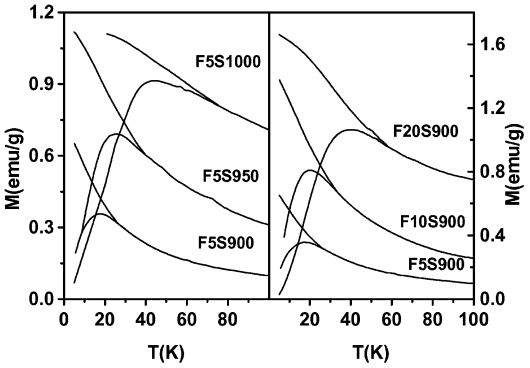

Figure 4. ZFC−FC magnetization curves as a function of temperature with an external applied field of 200 Oe.

with different composition but similar crystallite size, M_S values normalized to the γ-Fe_2O_3 content were similar (Table 1). The fact that all the characterized samples were superparamagnetic allows us to estimate the magnetic size distribution parameters following the method of Chantrell et al.,[23] which uses magnetic measurements at low and high fields to obtain a fit to a sum of Langevin equations and a log-normal distribution to describe the form of particle size distribution.[24] The average particle size determined with this method is similar to that determined by XRD and TEM.

To obtain qualitative information on the blocking temperature of the superparamagnetic composites, we registered the ZFC and FC curves as a function of temperature for all the samples (Figure 4). When the nanoparticles are cooled well below the blocking temperature without a magnetic field (ZFC), the magnetic moments in each single-domain nanoparticle point along their easy axis. The random packing of the particles results in the overall random-pointed magnetization of the individual nanoparticles. The total magnetization is very low because the applied magnetic field is not strong enough to overcome the magnetic anisotropy. On heating, the thermal energy overcomes the magnetic anisotropy in the smallest nanoparticles and therefore their moments start to align with the applied field (the total magnetization initially increases with increasing temperature). When the magnetization directions of almost all of the nanoparticles point to the field direction, a maximum in the ZFC is obtained. Above this temperature, the sample follows a typical paramagnetic behavior of decreasing magnetization as the temperature increases. It is generally assumed that the temperature of the ZFC maximum is directly proportional to the average blocking temperature, $T_M = \beta T_B$, where β is a constant depending on the shape of the size distribution.[25,26] It is clear that in all the samples a maximum is observed in the ZFC curves (Figure 4), which clearly indicates that the composites exhibit superparamagnetic behavior. An increase of the temperature at which the ZFC peak reaches its cusp, T_M, is evident as the γ-Fe_2O_3 crystallite size increases (Figure 4, Tables 1 and 2). Also, an increase in T_M is observed with the increase of packing fraction, which must be associated with an increase in the interparticle interactions.[27,28] Since the particles in the sample have a certain distribution of volumes, each one of them becomes blocked at a different temperature, giving rise to a distribution of blocking temperatures (broadening of the ZFC magnetization curve).

As the nanoparticles are cooled to very low temperatures in the presence of a magnetic field (FC), the magnetization direction of each particle is frozen in the field direction. Therefore, in the FC process the magnetization displays the highest value at the lowest registered temperature (5 K in our experiments). The temperature at which the ZFC and FC curves start to separate (T_S) corresponds to the blocking of the largest particles. The difference between T_S and T_M is therefore a qualitative measure of the width of the energy barrier distribution and, thus, of the nanoparticles size distribution.[26] This difference (Figure 4, Tables 1 and 2), in accordance with the results obtained with TEM, increased both with the iron oxide content and the heating temperature.

Figure 5 shows the reduced remanence data as a function of temperature for all the samples. We have analyzed the results using the standard relation for the temperature variation of the reduced remanence (normalized to the measured saturation magnetization),

Table 2. Values of T_M, T_S Obtained from the ZFC−FC Curves, $M_R(0)/M_S(0)$, $<T_B>$, σ_y Obtained from the Fit of the Decay of the Reduced Remanence, K_{Eff} Obtained from the Law of Approach to Saturation, and H_C Obtained from the Hysteresis Loops Registered at 5 K[a]

sample	T_M (K)	T_S (K)	$M_R(0)/M_S(0)$	$<T_B>$ (K)	σ_y (nm)	K_{eff} ($\times 10^6$ erg/cm^3)	H_C (Oe)
F5S900	17	25	0.32	8	0.95	3.7	386
F5S950	26	38	0.34	25	1.05	2.5	469
F5S1000	44	75	0.37	41	1.15	1.3	482
F10S900	22	32	0.30	13	1.05	3.9	460
F20S900	40	60	0.27	20	1.10	3.5	1450

[a] The uncertainties are about 0.02 for $M_R(0)/M_S(0)$, 0.1 for the standard deviation, 1−2 K for $<T_B>$, and 10−15% for the effective anisotropy constants.

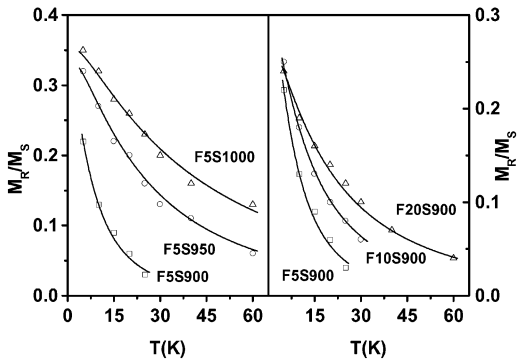

Figure 5. Variation of the reduced isothermal remanence with temperature for all the samples. The solid lines represent the best fit of the data with a standard decay-of-remanence model.

(23) Chantrell, R. W.; Popplewell, J.; Charles, S. W. *Physica* **1977**, *86−88B*, 1421.
(24) O'Grady, K.; Bradbury, A. *J. Magn. Magn. Mater.* **1983**, *39*, 91.
(25) Gittleman, J. I.; Abeles, B.; Bozoeski, S. *Phys. Rev. B* **1974**, *9*, 3891.
(26) Cannas, C.; Casula, M. F.; Concas, G.; Corria, A.; Gatteschi, D.; Falqui, A.; Musinu, A.; Sangregorio, C.; Spano, G. *J. Mater. Chem.* **2001**, *11*, 3180.
(27) El-Hilo, M.; O'Grady, K.; Chantrell, R. W. *J. Magn. Magn. Mater.* **1992**, *114*, 295.
(28) Mørup, S.; Bødker, F.; Hendriksen, P. V.; Linderoth, S. *Phys. Rev. B* **1995**, *52*, 287.

which allows us to obtain quantitative information about the mean blocking temperature. The relation is given by[27]

$$\frac{M_R(T)}{M_S(T)} = \frac{M_R(0)}{M_S(0)} \int_{T/<T_B>}^{\infty} f(y)\, dy \qquad (1)$$

where $<T_B>$ is the mean blocking temperature, $y = T_B/<T_B>$ is the reduced blocking temperature, and $M_R(0)/M_S(0)$ is the reduced remanence at 0 K. The distribution $f(y)$ of reduced blocking temperatures is assumed to be a log-normal function.

$$f(y) = \frac{1}{(2\pi)^{1/2}\sigma_y} \exp\left[-\frac{(\ln y)^2}{2\sigma_y^2}\right] \qquad (2)$$

The best fits with eq 1 to the data are shown by the lines in Figure 5, and the values of the free parameters $M_R(0)/M_S(0)$, $<T_B>$, and the standard deviation σ_y are given in Table 2. In the ideal case of well-separated fine particles with uniaxial anisotropy, the value of $M_R(0)/M_S(0)$ is 0.5; however, as the packing fraction increases, the interparticle dipolar attraction becomes comparable to the magnetic anisotropy energies. The competition between the interactions and the anisotropy of the individual γ-Fe_2O_3 nanocrystals produces frustration,[29] which decreases the value of $M_R(0)/M_S(0)$ (Table 2). In accordance, this ratio decreased with increasing iron oxide concentration (Table 2). For the samples with the same iron oxide content (i.e., same volume packing fraction), a slight increase in the value of $M_R(0)/M_S(0)$ was detected with increase of the heating temperature (i.e., increase in crystallite size), which can also be explained in terms of decreasing interparticle interactions as the particle size increases. The separation distance, D, between particles is not only a function of the volume packing fraction, X, but also of the particle size, d. Roughly, it can be expressed by $D = d(1/X^{1/3} - 1)$. Therefore, for a given volume packing fraction, the separation distance increases with the increase in particle size (i.e., decrease in interparticle interactions).

The values of $<T_B>$ (Table 2) increased with increase of both particle size and iron oxide content (i.e., increase of interparticle interactions). Even though the decay of remanence is mainly determined by the anisotropy,[27] the distribution in barriers height is also modified by the presence of interparticle interactions,[28] which could explain the observed increase in $<T_B>$ with the iron oxide content. The other parameter obtained from the fit that could provide information about the size distribution of the magnetic nanocrystals dispersed in the silica matrix is the standard deviation σ_y (Table 2). As observed, this value increased with both the particle size (i.e., heating temperature) and iron oxide content. This result agrees to that previously obtained from TEM and the ZFC−FC curves.

Values of the effective magnetic anisotropy of the particles, K_{eff}, can provide information about the existence in addition to the magnetocrystalline anisotropy of other anisotropy terms, say, for example, surface and interface anisotropy. Attempts were made to calculate this value from the magnetization data at 5 K using the law of approach to saturation:[30]

$$M = M_S\left(1 - \frac{B}{H^2} - \frac{C}{H^3}\right) + \chi_f H \qquad (3)$$

where M_S is the saturation magnetization, χ_f is the high-field susceptibility, and B is a function of M_S and K_{eff}. For uniaxial polycrystalline structures, B is given by the following expression.[31]

$$B = 4S_B K_{eff}^2/15M_S^2 \qquad (4)$$

where S_B is a measure of the volume fraction of blocked particles at a given temperature (5 K in this case), $S_B = [M_R(5)/M_S(5)]/[M_R(0)/M_S(0)]$.[32] $M_R(5)/M_S(5)$ was obtained from the hysteresis loop registered at 5 K, and $M_R(0)/M_S(0)$ was obtained from the above-determined fit of the reduced remanence data.

The obtained values (Table 2) are ~2 orders of magnitude larger than the bulk magnetocrystalline anisotropy constant ($K \approx 4.7 \times 10^4$ erg/cm^3), which clearly indicates that the enhancement can be considered basically as coming from either surface or interface anisotropy contributions.[33] The fact that the values of K_{eff} were similar for the samples with different volume packing fractions but similar particle size (Tables 1 and 2) supports this interpretation. In our system, shape anisotropy can be disregarded because the nanocrystals are essentially spherical. For coherent magnetization reversal of randomly oriented γ-Fe_2O_3 particles, values of the coercivity field of ~75 Oe are expected.[34] The values of H_C registered at 5 K (Table 2) are in all cases much higher than this value, which indicates that the reversal process is not controlled only by magnetocrystalline anisotropy but rather by surface or interface anisotropy. The presence of a disordered surface layer that freezes below ~30 K has been associated with the significant enhancement of coercivity field values.[1(d)] As observed, the values of H_C increased with the increase of the iron oxide content, which could be related to the presence of interparticle interactions.

Conclusions

It has been shown that tunable superparamagnetic nanocrystals dispersed in submicrometer diamagnetic matrixes can be obtained from microemulsions containing high element concentrations. Essential to the preparation were the presence of residual carbonaceous species and the heating temperature. We have determined that the magnetic response of these composites depends not only on the volume of the magnetic unit but also on the degree of dispersion of the magnetic nanocrystals within the diamagnetic matrix. We have also determined that interparticle interactions cause frustration of the moments. Finally, we have concluded

(29) Held, G. A.; Grinstein, G.; Doyle, H.; Sun, S.; Murray, C. B. *Phys. Rev. B* **2001**, *64*, 012408.

(30) Cullity, B. D. In *Introduction to Magnetic Material*; Addison-Wesley: Reading, MA, 1972; p 347.

(31) Kojima, H. In *Ferromagnetic Materials*; Wohlfarth, E. P., Ed.; North-Holland: Amsterdam, 1982; Vol. 3.

(32) Martinez, B.; Roig, A.; Molins, E.; González-Carreño, T.; Serna, C. J. *J. Appl. Phys.* **1998**, *83*, 3256.

(33) Prené, P.; Tronc, E.; Jolivet, J. P.; Livage, J.; Cherkaoui, R.; Nogues, M.; Dorman, J. L. *IEEE Trans. Magn.* **1993**, *29*, 2658.

(34) Bates, G. In *Ferromagnetic Materials*; Wohlfarth, E. P., Ed.; North-Holland: Amsterdam, 1980; Vol. 2, p 442.

that the enhancement of effective magnetic anisotropy with respect to the bulk γ-Fe_2O_3 can be considered as coming fundamentally from surface anisotropy.

Acknowledgment. Financial support from CICYT (PB98-0525) and Pacti (COO1999-AX011) is gratefully acknowledged.

The paper reports a simple and versatile method to prepare superparamagnetic composites using microemulsions with a high content in the magnetic precursor. The composites so obtained have been crystallochemically and magnetically characterized.

CM021214D